Effects of chemical and processing variables on paclitaxel-loaded polymer nanoparticles prepared using microfluidics

Aman Bains & Matthew G. Moffitt

December 2017

The final publication is available at:

https://doi.org/10.1016/j.jcis.2017.08.053

Citation for this paper:

Bains, A., & Moffitt, M. G. (2017). Effects of chemical and processing variables on paclitaxel-loaded polymer nanoparticles prepared using microfluidics. *Journal of Colloid and Interface Science*, 508, 203-213. https://doi.org/10.1016/j.jcis.2017.08.053.

Effects of Chemical and Processing Variables on Paclitaxel-Loaded Polymer Nanoparticles Prepared Using Microfluidics

Aman Bains and Matthew G. Moffitt*

Department of Chemistry, University of Victoria, P.O. Box 3065, Victoria, BC, Canada V8W 3V6

Abstract

For paclitaxel (PAX)-loaded polymeric nanoparticles PNPs prepared in a two-phase gas-liquid microfluidic reactor, the effects of microfluidic flow rate on the multiscale structure, loading efficiency and release rate are determined for three different copolymer compositions and two orders of magnitude variation in the PAX loading ratio. All experiments are carried out in the limit of low drug-to-polymer loading ratios ($r \leq 0.01$, w/w). In this range of r, PCL crystallinity, loading efficiency and release rate are not significantly affected by the amount of PAX dissolved in the core. These results are in sharp contrast to microfluidic PNPs prepared in a range of high loading ratios ($r \geq 0.1$), where the amount of added PAX has a strong influence on the multiscale structure and properties of drug delivery PNPs. For the case of $r = 0.01$, we show that flow rate strongly affects PNP morphologies for all three block copolymer compositions. For the shortest and longest PCL block lengths, the relative number of cylindrical morphologies increases and then decreases with increasing flow rate, whereas for the intermediate PCL block length, the number of cylinders steadily increases as the flow rate increases. Internal PCL crystallinities and PAX loading efficiencies show similar trends, both parameters increasing and decreasing with increasing flow rate for the extreme PCL block lengths and steadily increasing for the intermediate PCL block length. PAX release profiles indicate a marked slowing of PAX release as either the PCL block length or the microfluidic flow rate increase. Working in the limit of low loading ratio, this work provides clarity on separating the relative effects of copolymer composition and processing along with perturbations caused by the molecular cargo on the structure and function of drug delivery PNPs. These critical insights thus inform controlled microfluidic preparation of more medically-relevant PNPs at higher therapeutic loading levels.

Introduction

Amphiphilic block copolymers undergo self-assembly in selective solvents to form polymeric nanoparticles (PNPs) with promising properties for drug delivery applications.[1-20] These applications require fine control of the multiscale structure of PNPs on various disparate length scales.[16,21-32] For example, PNP size and morphology (~10-100 nm) are found to strongly influence biodistribution (e.g. via the enhanced permeability and retention effect in tumours) and circulation time,[16,24,25,27] while the internal crystallinity of PNPs (~1-10 nm) is a critical factor of particle stability, flexibility, loading efficiency, and release rate.[22,23,33-35] Although most research on amphiphilic block copolymer self-assembly focuses on varying the multiscale structure through changes in chemical conditions (e.g. copolymer composition, concentration, and solvent),[36-40] other studies have shown that external forces (e.g. shear or confinement) can be applied to direct size, morphology and internal crystallinity of PNPs, allowing specific nanostructures to be "dialled in" through changes in processing conditions without having to change the chemical conditions of the formulation.[33-35,41-43]

In our group, we have shown that localized high-shear "hot spots" within segmented gas-liquid microfluidic reactors[44] enable flow-directed multiscale structure in various PNP systems, including polymer-quantum dot colloidal assemblies,[41,42] PNPs of polystyrene-*block*-poly(acrylic acid) (PS-*b*-PAA),[43,45-47] photoactive block copolymer PNPs,[48] and drug delivery PNPs of biocompatible polycaprolactone-*block*-poly(ethylene oxide) (PCL-*b*-PEO).[33-35,49] In these various polymer systems, we have demonstrated continuous variability of PNP structure on multiple length scales, including size and morphology, and the internal crystallinity of the hydrophobic cores, simply by changing the flow rate during microfluidic manufacturing. We have also shown that for PNPs of the semicrystalline copolymer PCL-*b*-PEO loaded with the

anti-cancer agent paclitaxel (PAX), processing control of multiscale structure *via* microfluidics enables tuning of drug delivery function,[33] including drug loading efficiencies,[33-35] release rates,[33-35] and antiproliferative potencies against human breast cancer MCF-7 cell line.[35]

In this paper, we present a detailed study of the effects of flow rate on the multiscale structure, loading efficiency and release rate of microfluidic-prepared PAX-loaded PNPs for three different copolymer compositions and two orders of magnitude variation in the PAX loading ratio. Unlike previous studies from our group on microfluidic PAX encapsulation at high loading ratios of $r \geq 0.1$,[33,35] this study is undertaken in the limit of low loading ratios ($r \leq 0.01$), where we show that PCL crystallinity, loading efficiency and release rate are not strongly affected by the amount of PAX dissolved in the core; however, all of these parameters are found to depend strongly on the flow rate and block copolymer composition. This is in sharp contrast to our recent study of microfluidic PNPs prepared in a range of high loading ratios ($r \geq 0.1$),[35] where the amount of added PAX has a strong influence on the multiscale structure and properties of drug delivery PNPs. By investigating a regime of drug loading in which drug delivery properties are strongly influenced by microfluidic processing but not on the amount of drug, this work provides information toward disentangling the effects of processing on the structure and function of PNPs from the effects of the added molecular cargo. Such insights are critical for the preparation of more medically-relevant PNPs at higher therapeutic loading levels. The results also show that both the block copolymer composition (in particular the length of the PCL block) and flow rate provide complementary chemical and processing handles, respectively, on reproducible variation of structure and function of PAX-loaded PNPs.

Experimental

Materials. Three different poly(ε-caprolactone)-*block*-poly(ethylene oxide) (PCL-*b*-PEO) copolymers with constant PEO block length and variable PCL block lengths were purchased from Advanced Polymer Inc. and used as received: PCL_{12k}-*b*-PEO_{5k} (PCL(12k)); $PCL_{6.4k}$-*b*-PEO_{5k} (PCL(6.4k)) and $PCL_{2.1k}$-*b*-PEO_{5k} (PCL(2.1k)) where numbers in subscripts refer to number-average molecular weights of the respective blocks. *N*,*N*-dimethylformamide (DMF) (Aldrich, 99.9+%, HPLC grade, H_2O < 0.03%), paclitaxel (PAX, Polymed Therapeutics, Inc.), methyl *tert*-butyl ether (Sigma-Aldrich) and bovine serum albumin (Sigma Aldrich), were used as received without further purification.

All quantitative stock solutions of PCL-*b*-PEO and PAX in DMF were prepared gravimetrically by accurately weighing the solid(s) into clean glass vials followed by gravimetric addition of a known quantity of DMF; all stock solutions were equilibrated overnight with stirring before further use.

Critical Water Content Determination. Static light scattering (SLS) measurements were carried out to determine the critical water content (cwc) of 0.33 wt % DMF solutions of PCL-*b*-PEO, which was the initial condition for all self-assembly experiments in this study. SLS measurements were carried out using a Brookhaven Instruments photon correlation spectrometer equipped with a BI-200SM goniometer, a BI-9000AT digital autocorrelator, and a Melles Griot He-Ne Laser (633 nm) with a maximum power output of 75 mW.

A 1.0 wt % stock solution of PCL-*b*-PEO in DMF was filtered through a Teflon syringe membrane filter with a nominal pore size of 0.45 μm (VWR) into precleaned scintillation vials. The filtered stock was then diluted to 0.33 wt % by gravimetric addition of the required quantity of DMF. To the resulting ~6 g of solution, deionized water was added in successive 0.03-0.06 g

quantities *via* a microsyringe equipped with two membrane filters (VWR) with nominal pore size of 0.20 μm connected in series. After each addition of water, the solution was agitated using a vortexer to aid in mixing. The solution was then allowed to equilibrate for 15 min before measuring the scattered light intensity. All measurements were carried out at a scattering angle of 90° and a temperature of 23 °C. From the resulting plot of scattered light intensity versus weight percentage of added water, the cwc was determined from the intercept of linear fits to the baseline and the region of the plot in which scattered light intensity increased sharply (above the cwc). Determinations of cwc were carried out three times from the same stock solution and the mean value and standard deviation of the three measurements were used to calculate the reported cwc and experimental error. The cwc values for PCL(12k), PCL(6.4k), and PCL(2.1k) are 5.5 ± 0.4 wt %, 6.3 ± 0.2 wt %, and 13.1 ± 0.2 wt %, respectively.

Microfluidic Chip Fabrication. Negative masters were fabricated on high quality silicon wafers (Silicon Quest International, Santa Clara, CA) using the negative photoresist SU-8 100 (Microchem Inc.). Immediately prior to use, the wafers were heated on a hot plate at 200 °C for 20 minutes to remove moisture. A 150 μm-thick SU-8 film was spin-coated onto the silicon and then heated to 95 °C for 60 minutes to remove residual SU-8 solvent. A photomask was then placed over the SU-8 film and exposed to UV light for 180 s. Then, the UV-treated film was heated at 95 °C for 20 min before submersion in SU-8 developer (Microchem) until all unexposed photoresist was removed.

Microfluidic chips were fabricated from poly(dimethylsiloxane) (PDMS) using a SYLGARD 184 silicon elastomer kit (Dow Corning, Midland, MI). For chips used in the preparation of PAX-loaded PNPs, elastomer base-to-curing agent ratios of 7:1 and 20:1 for the substrate and channel layers, respectively, were used. For fabrication of all PDMS chips, the

elastomer and curing agent were mixed together and degassed in a vacuum chamber. The degassed PDMS was then poured over the negative master in a Petri dish and further degassed until all remaining air bubbles were removed. The PDMS was then heated at 85 °C for ~60 min until cured. The microfluidic chip was then peeled off of the negative master and holes were punched through its reservoirs to allow for the insertion of tubing. A thin PDMS film (substrate layer) was also formed on a glass slide by spin-coating and was permanently bonded to the base of the microfluidic reactor (channel layer) after both components were exposed to oxygen plasma for 60 s. The reactor has a set channel depth of 150 μm and consists of a sinusoidal mixing channel 100 μm wide and 18 mm in length and a sinusoidal processing channel 200 μm wide and 740 mm in length.

For further stabilization of the bubble generation process, an external resistor chip was used between the Ar gas tank and the microfluidic chip. The resistor chips served as high pressure drop systems to efficiently dampen the pressure fluctuations caused by the Ar gas tank and the bubble generation process. The total pressure drop in the external resistor chip was sufficient to suppress pressure fluctuations within the Ar line. The resistor chip channels were 1000 mm long, 150 μm deep and 400 μm wide.

PDMS is chosen as a convenient reactor material due to its relatively facile fabrication. It is important to note that PDMS has a tendency to swell in come solvents also to undergo adhesion with organic materials, both of which can be concerns for microfluidic preparation of PNPs. In our group, we have compared several solvents for PNP preparation in PDMS reactors and found that neither dioxane nor DMF lead to significant microchannel swelling and that reactors can be used and reused with these solvents and their mixtures with water. However, THF is found to significantly swell the PDMS reactor and preclude the use of this common

solvent for PNP preparation. Adhesion of material to the channel walls during PNP manufacturing cannot be ruled out, although significant clogging of the channels has only be observed for the PCL(12k) copolymer, and only at higher r values than are described in this paper. To mitigate contamination due to wall adhesion of material from pervious microfluidic runs, the reactors are flushed well with the relevant solvent mixtures before they are applied to PNP preparation.

Flow Delivery and Control. Pressure-driven flow of liquids to the reactor inlet was provided using 1 mL gastight syringes (Hamilton, Reno, NV) mounted on syringe pumps (Harvard Apparatus, Holliston, MA). The microchip was connected to the liquid syringes via 1/16th-inch (OD) Teflon tubing (Scientific Products and Equipment, ON). Gas flow was introduced to the microchip via an Ar tank regulator and a downstream regulator (Johnston Controls) for fine adjustments. The microchip was connected to the downstream regulator through a 1/16th-inch (OD) / 100-μm (ID) Teflon tube (Upchurch Scientific, Oak Harbor, WA). The liquid flow rate (Q_{liq}) was programmed via the syringe pumps and the gas flow rate (Q_{gas}) was fine-tuned via the downstream pressure regulator in order to dial in the nominal total flow rates described in the main text. Due to the compressible nature of the gas and the high gas/liquid interfacial tension, discrepancies arise between the nominal (programmed) and actual values of Q_{gas}, Q_{gas}/Q_{liq}, and the total flow rate (Q_{total}). Therefore, actual gas flow rates were calculated from the frequency of bubble formation and the average volume of gas bubbles, determined from image analysis of the mean lengths of liquid and gas plugs, L_{liq} and L_{gas}, respectively, under a given set of flow conditions. This method of flow calculation has been previously employed in the context of gas-liquid segmented flow in the microfluidic device. For all experiments, the relative gas-to-liquid flow ratio, Q_{gas}/Q_{liq} ~1 and all actual Q_{total} values are within 10% of

nominal values reported in the main text. Visualization of the gas bubbles and liquid plugs within the microfluidic reactor was achieved using an upright optical microscope (Omax) with a 10×-objective lens. Images were captured using a 2.07 megapixel PupilCam (Ken-A-Vision) and mean lengths of liquid and gas plugs were determined from the images using image analysis software (ImageJ).

Microfluidic Preparation of PAX-Loaded PCL-*b*-PEO PNPs. For experiments probing the effect of copolymer composition and drug concentration on microfluidic assembly of PAX-loaded PCL-*b*-PEO PNPs, three fluid streams were combined at equal flow rate to form gas-segmented liquid plugs within the reactor: (1) for copolymer composition experiments: 1.0 wt % solution of PCL-*b*-PEO (PCL(12k), PCL(6.4k), and PCL(2.1k)) in DMF with codissolved PAX in drug : copolymer ratio, *r*, of 0.01 (w/w); for drug concentration experiments: 1.0 wt % solution of PCL-*b*-PEO (PCL(12k)) in DMF with codissolved PAX in drug : copolymer ratios of *r* = 0.001, 0.005, 0.0001, and 0.0005 (w/w), (2) a separator stream containing DMF only, and (3) a DMF solution containing deionized water; the water concentration was (cwc + 5 wt %) × 3. Combination of the three liquid streams yielded steady-state on-chip concentrations of 0.33 wt % copolymer and cwc + 5 wt% deionized water. Microfluidic flow conditions were selected and controlled as described in the previous section. All microfluidic experiments were carried out at ambient room temperature within 1-2 days to minimize temperature variability and accompanying changes in solution viscosities.

The PAX-loaded PNP samples were collected from the reactor into vials containing a 10×-excess volume of deionized water, determined with respect to the volume of PNP dispersion collected from the reactor based on the flow rate and collection time. This quenching step was followed by 12 h dialysis against deionized water (with changing of water every hour for the first

4 h of dialysis) to remove residual DMF and unencapsulated PAX. The resulting aqueous dispersions of PAX-loaded PNPs were analyzed by TEM, XRD, and also used for studies of PAX loading efficiencies and release kinetics, as described in the corresponding sections below. All samples were prepared in triplicate under the specified chemical and flow conditions.

An important question about the above quenching and dialysis steps is their possible effects on the structure and properties of the formed PNPs. We carried out experiments on selected microfluidic preparations (PNPs from PCL(12k) without loaded PAX prepared at various on-chip water contents and flow rates; Supporting Information, Figure S3) and found minimal differences in PNP morphologies comparing unquenched samples (collected directly from the chip without dilution) with those that had been quenched and dialyzed. However, since dilution and dialysis is a required step for preparing drug-loaded PNPs, in order to remove the excess, encapsulated drug from the sample, we could not make such a comparison for the drug-loaded samples described in the paper. The data in Figure S3 suggest that core crystallites formed in the reactor before dilution act as crosslinks which maintain structural integrity of the PNPs during quenching and dialysis, although we cannot be certain that such crosslinks prevent structural rearrangements of the PAX-loaded PNPs. However, the observed flow-rate dependences following quenching and dialysis indicate that the shear history of the on-chip preparation is not erased by any possible rearrangements. Since the goal of the method is to establish correlations between the controllable flow during manufacturing and the off-chip PNP properties after quenching and dialysis, as long as this shear history is retained and some of the shear-directed final properties are interesting/applicable, then the method is a viable platform for processing control of nanomedicine materials.

Bulk Preparation of PAX-Loaded PCL-*b*-PEO PNPs. Off-chip PAX-loaded PCL-*b*-PEO PNPs were prepared by a conventional drop-wise water addition method described elsewhere in the literature.[1,35] Initial conditions for self-assembly were kept identical to the on-chip formulations. Approximately 5 mL of 0.33 wt % copolymer solution was prepared in DMF at a drug : copolymer ratio of 0.01 (w/w) and water was added drop-wise using a micropipette at a constant rate of 20 μL every 10 s with moderate magnetic stirring (~600 rpm). Drop-wise water addition at constant rate was continued to a water content of cwc + 5 wt %, then the drug-loaded PNPs were quenched immediately into 10x-volume excess of deionized water, followed by 12 h dialysis against deionized water (250× excess; with changing of water every hour for the first 4 h of dialysis) to remove residual DMF and unencapsulated PAX. The resulting aqueous dispersions of PAX-loaded PNPs were analyzed by TEM, XRD, and also used for studies of PAX loading efficiencies and release kinetics, as described in the corresponding sections below. All samples were prepared in triplicate under the specified conditions. It should be noted that a large number of non-microfluidic (bulk) preparation methods for PNPs have been described in the literature and the choice of preparation method has been shown to have a strong influence on the PNP structure and properties due to strong contributions from kinetic effects.[50-53] The above method was chosen as a "bulk control" in this study for two reasons. First, drop-wise water addition has been applied extensively in the literature, especially in early studies of amphiphilic block copolymer self-assembly,[36-40] since PNPs formed by slow water addition will generally be closer to thermodynamic equilibrium than those formed by fast water addition.[54] Second, the formation kinetics of bulk-PNPs formed by slow water addition provide a sharp contrast to those formed by microfluidic mixing in which water reaches its steady-state concentration in < 1 s.[41]

Transmission Electron Microscopy. Transmission electron microscopy (TEM) was performed using a JEOL JEM-1400 TEM, operating at an accelerating voltage of 65 kV and equipped with a Gatan Orius SC1000 CCD camera. TEM images were obtained by depositing diluted dispersions (~0.03 wt % copolymer) consisting of PAX-loaded PCL-*b*-PEO PNPs in water onto carbon-coated 300 mesh copper TEM grids as described below.

To improve contrast, uranyl acetate was used to negatively stain the PCL-*b*-PEO PNPs. Uranyl acetate selectively binds to the PEO coronal chains, providing reverse contrast for the PCL cores, which appear white in TEM images of stained samples.[26,55] For reverse staining experiments, PNP dispersions were mixed with 1 wt % aqueous solution of uranyl acetate in a 1:1 ratio (v/v) and one drop of the resulting mixture was deposited onto a TEM grid. Excess liquid was immediately removed using lens paper, followed by drying of remaining liquid under ambient conditions.

Dynamic Light Scattering. Effective hydrodynamic diameters of PAX-loaded PCL-*b*-PEO PNPs were determined using dynamic light scattering (DLS). DLS measurements were carried out using a Brookhaven Instruments photon correlation spectrometer equipped with a BI-200SM goniometer, a BI-9000AT digital autocorrelator, and a Melles Griot He-Ne Laser (633 nm) with a maximum power output of 75 mW. All DLS measurements of PAX-loaded PNPs were performed in pure water and an experimental temperature of 23˚C and at a scattering angle of 90˚.

After overnight dialysis against deionized water to remove residual DMF and unencapsulated PAX, the PAX-loaded PNPs were transferred to pre-cleaned scintillation vials then diluted 5x using deionized water, filtered through two nylon syringe filters in series with nominal pore sizes of 0.2 μm (National Scientific Company) to give a final copolymer

concentration of ~0.07 mg/mL. For each PNP preparation, mean effective hydrodynamic sizes were determined from three measurements of the autocorrelation function using cumulent analysis. Mean effective hydrodynamic diameters were determined from three separate data collections corresponding to one individually-prepared stock solution, such that reported errors reflect the error in data collection.

X-Ray Diffraction. X-ray diffraction measurements were performed on a Rigaku Miniflex diffractometer with a Cr source (kR radiation, λ = 2.2890 Å) operating at 30 kV and 15 mA with a resolution of 0.05° (2θ) and a scan speed of 1°/min. X-ray diffraction profiles were collected for 2θ ranging from 10-80 degrees.

For XRD sample preparation, water was removed from suspensions of PAX-loaded PNPs by rotary evaporation at 25 °C until solid films were obtained. The resulting films were then scraped as a powder into the XRD specimen holder with no subsequent drying step to remove residual solvent. We note that this preparation method will significantly increase the crystallinity of coronal PEO blocks relative to their colloidal state, as removal of water from the PNP coronae will allow initially-solubilized PEO chains to pack together. However, since the hydrophobic cores will contain no water in the purely aqueous suspensions, we do not expect the crystallinity of the core-forming PCL blocks to be strongly affected when water is removed by rotary evaporation. Therefore, our XRD experiments should provide a reasonable probe of PNP core crystallinity in the colloidal state.

Peak deconvolution of XRD data was done using Origin Pro Version 8.1. Two characteristic reflections for each of crystalline PCL and crystalline PEO were identified from the literature and these were used to fix the positions of four Lorentzian peak contributions to the fit; another small Lorentzian peak contribution was used to account for a small shoulder on the

more intense PCL peak in order to obtain a good fit. Thus, XRD data were fit to a sum of 6 Lorentzian functions: 3 peaks assigned to crystalline PCL (2θ = 32.5, 32.7, and 35.7), 2 peaks assigned to crystalline PEO (2θ = 29.2, 35.4), and 1 peak (no fixed position) assigned to incoherent scattering from amorphous copolymer (amorphous halo). Areal peak contributions from the three components (crystalline PCL, crystalline PEO, and amorphous copolymer) were then determined by integration and percentages of crystalline PCL and PEO were calculated using:

$$\%\ Crystalline\ \text{PCL} = A_{\text{PCL}}/A_{\text{total,}}\ \text{and}\ \%\ Crystalline\ \text{PEO} = A_{\text{PEO}}/A_{\text{total}},$$

where $A_{\text{total}} = A_{\text{PCL}} + A_{\text{PEO}} + A_{\text{amorph.}}$

PAX Loading Efficiency Determination. To determine PAX loading efficiencies, PAX-loaded PNPs were dissolved in acetonitrile (ACN): First, water was removed from a known mass (~1 g) of an aqueous dispersion of PAX-loaded PNPs of known copolymer concentration by rotary evaporation at 25 °C; then a known amount (~0.5 g) of ACN was added to break up the PAX-loaded PNPs by stirring in ACN for 4 h. PAX quantification was conducted using high performance liquid chromotography-mass spectrometry (HPLC-MS, Ultimate 3000, Thermo Scientific) with a C18 column (Phenomenex Luna 5u C18) and a mobile phase composition of 65/35 acetonitrile/water (v/v) and 1 vol % formic acid using the diode array detector (DAD). Sample injection volumes were 50 μL and the HPLC-MS flow rate was set to 1 mL/min. For loading efficiency determinations, PAX solution concentrations were sufficiently high such that they could be detected and quantified using the diode array detector (DAD) by monitoring the elution of PAX at a characteristic absorption wavelength of 227 nm. A calibration curve for the DAD was generated by analysis of 5 stock solutions containing different known PAX concentrations in ACN. Calibration of the DAD detector yielded a limit of detection (LOD) and

limit of quantification (LOQ) for PAX of 54 ppm and 163 ppm, respectively. Quantities of PAX in the various dissolved PNP solutions were determined and loading efficiencies calculated for each sample using the following expression:

$$loading\ efficiency\ (\%) = \frac{PAX\ in\ micelles\ (g)}{total\ PAX\ used\ (g)} \times 100\%$$

Reported loading efficiencies are averages determined from triplicate PNP preparations under the specified conditions.

***In Vitro* PAX Release Kinetics.** Experiments were carried out to monitor the *in vitro* release of PAX from PAX-loaded PNPs using HPLC-MS (see previous section for instrument specifications). In a typical experiment, an aqueous dispersion of PAX-loaded PNPs (~10 g) were transferred to a 10 mL-dialysis bag (SpectrumLabs, MWCO 100 kDa), which was placed in a 4 L-beaker containg the release medium. The release media consisted of ~2.5 L of a 1% phosphate buffer saline (PBS, pH = 7.4) solution containing albumin (Sigma Aldrich) at a concentration of 45 g/L; throughout release experiments, the release medium was constantly stirred using magnetic stirring and maintained at physiological temperature (37 °C) in an incubator. At predetermined times, aliquots of known mass (~1 g) were removed from the dialysis bag to which a known mass (~150 mg) of a deuterated PAX internal standard (d5-PAX, ~1 mg/mL, Toronto Research Chemicals) in ACN was added. A liquid-liquid extraction was conducted using methyl tert-butyl ether (Sigma Aldrich) to extract PAX from the aqueous solution. Methyl tert-butyl ether was then removed by rotary evaporation at 25 °C. Acetonitrile was then added to solubilized PAX before injection into the HPLC-MS.

The amount of PAX released was quantified using HPLC-MS on single ion monitoring (SIM) mode. Separate calibration curves for SIM detection of PAX and the internal standard

were generated by analysis of five known stock solutions of both analytes. Calibration of the SIM detector yielded a LOD and LOQ for PAX of 2 ppm and 5 ppm, respectively, and a LOD and LOQ for the internal standard of 2 ppm and 6 ppm, respectively. The internal standard (d_5-PAX) was used to determine the efficiency of each liquid-liquid PAX extraction, which was found to vary from 60-80%. From determined masses of PAX in aliquots obtained at different release times, percentages of PAX released were calculated relative to the determined mass of PNP-encapsulated PAX at the $t = 0$ release time. Reported release percentages at each release time are averages determined from triplicate PNP preparations under the specified conditions.

Results and Discussion

Effect of Flow Rate and Block Copolymer Composition on the Multiscale Structure of PAX-Loaded PNPs. We first explored how both copolymer composition and flow rate influence PAX-loaded PCL-*b*-PEO PNP multiscale structure (size, morphology and core crystallinity). Self-assembly and PAX encapsulation were conducted at constant PAX loading ratio ($r = 0.01$) for three different block copolymers (PCL(2.1k), PCL(6.4k) and PCL(12k)) and five different flow rates (Q = 0, 25, 50, 100 and 200 μL/min), where $Q = 0$ designates the bulk PNP preparation.

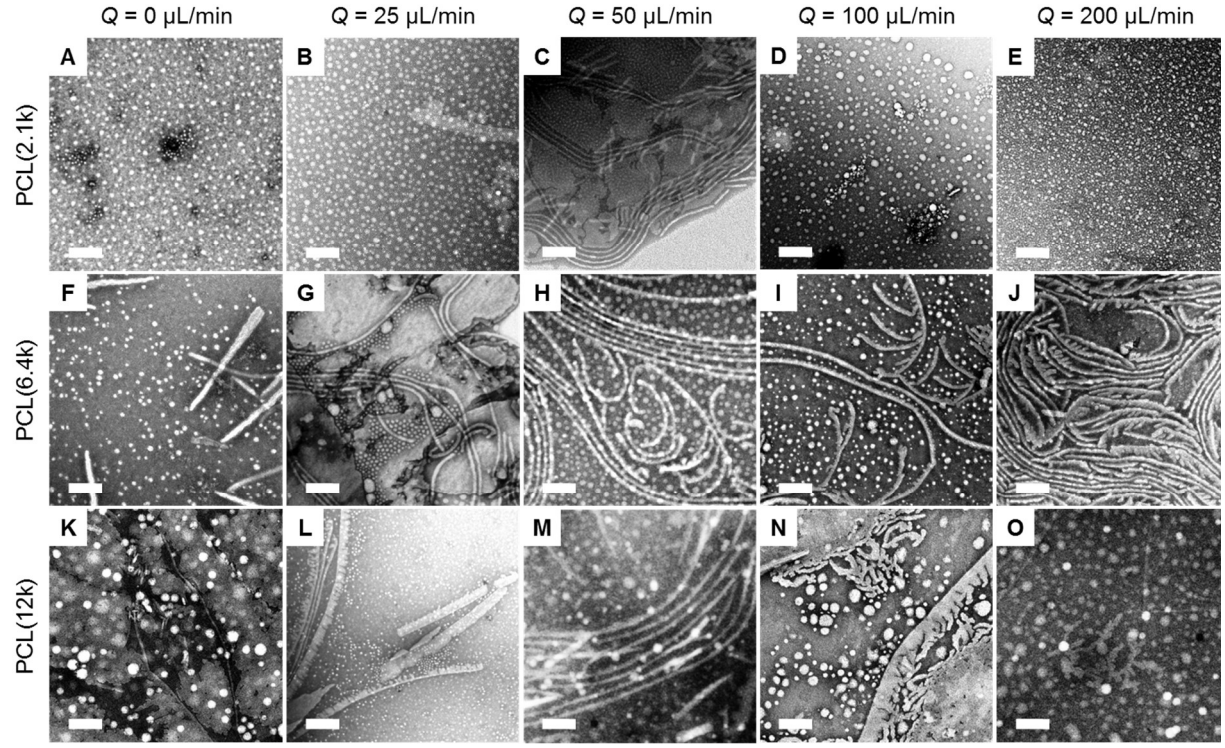

Figure 1. Effect of flow rate and copolymer composition on morphology of PAX-loaded PCL-*b*-PEO PNPs. TEM images were produced by negative staining with uranyl acetate. All scale bars are 200 nm.

Figure shows TEM data for the PAX-loaded PCP-*b*-PEO PNPs prepared from three block copolymers and five flow rates; DLS hydrodynamic size distributions are presented in Supporting Information (Figure S1). In general, both the PCL(2.1k) and PCL(12k) samples yield increasing numbers of cylinders with increasing flow rate up to a maximum flow rate, followed by a reversal of the trend, with the highest flow rate (Q = 200 µL/min) producing mostly spherical morphologies. In contrast, the PCL(6.4k) sample continues to yield increasing numbers of cylinders with increasing flow rate up to the highest investigated flow rate of Q = 200 µL/min. These complex and nonmonotonic trends in morphology with respect to flow rate are attributed to the competition of three different mechanisms of PNP processing within the microfluidic channels:[33] 1. shear-induced particle coalescence, 2. shear-induced particle breakup, and 3.

shear-induced crystallization. Which of these three mechanisms predominates at a given flow rate will depend strongly on the PCL block length, explaining the very different flow-dependent behaviours of the three copolymers.

Considering the effect of PCL block length on the PNP morphologies at the various flow rates (Figure 1), we find the strongest influence of PCL block length for the bulk preparations (Q = 0 μL/min), which we attribute to the absence of external shear forces and the predominance of intermolecular forces (Figure 1, A, F, and K). In these cases, with increasing PCL block length, PNP morphologies trend towards lower-curvature morphologies, exemplified by the transition from spheres (Figure 1A, PCL(2.1k)), to cylinders and spheres (Figure 1F, PCL(6.4k)), to lamellae and spheres (Figure 1K, PCL(12k)) as the molecular weight of the core forming block is increased. Similar trends of decreasing PNP curvature with increasing PCL block length are also found in the microfluidic preparations at Q = 25 μL/min where external shear forces are present but relatively weak (Figure 1, B, G, and L). However, for microfluidic preparations at the highest flow rates (Q > 25 μL/min) we do not find clear trends between the curvature of the predominant morphologies and the PCL block length. For instance, in the Q = 200 μL/min cases (Figure 1, E, J, and O), the morphologies go from spheres, to cylinders, then back to spheres as the PCL block length increases. These more complex trends at high flow rate indicate the complicated contributions of external shear forces which become increasing predominant as the flow rate in the microfluidic channels increases.

We previously carried out 2-week and 1-month storage stability tests (storage at 4°C under quiescent conditions) of PNPs formed from the PCL(12 k) copolymer at various microfluidic flow rates without quenching and dialysis to remove DMF, in order to determine the extent to which shear-directed morphologies relaxed over time in the absence of shear.[33] In that study, we

showed that the morphologies were entirely stable for at least 1-month of storage time except when stored at the lowest investigated water contents (cwc + 2 wt % in that study).[33] This stability was attributed to PCL crystallites within the core acting as physical crosslinks except when the DMF content was high enough to attenuate crystallite formation. For quenched and dialyzed PNPs such as those investigated here, no DMF remains in the dispersions such that crystallite formation should lead to even higher stability at 4°C than shown previously without quenching and dialysis. Long-term stability studies of quenched and dialyzed PNPs formed on-chip at various therapeutic PAX loading levels ($r \geq 0.1$), such as those discussed in a recent publication from our group,[35] are critical to developing the microfluidic approach as a viable drug delivery manufacturing platform; those studies will be discussed in an upcoming publication.

Next, we consider how the internal structure of PAX-loaded PNPs (r = 0.01), in the form of PCL core crystallinity, is influenced by PCL block length and flow rate (Figure 2). The data in Figure 2 present two main trends: 1. at each flow rate, PCL crystallinity generally increases with increasing PCL block length and 2. for a given PCL block length, PCL crystallinity for microfluidic-prepared PNPs ($Q > 0$) generally increases with flow rate, except at the highest flow rate for the PCL(2.1k) and PCL(12k) copolymers where a decrease in crystallinity is observed.

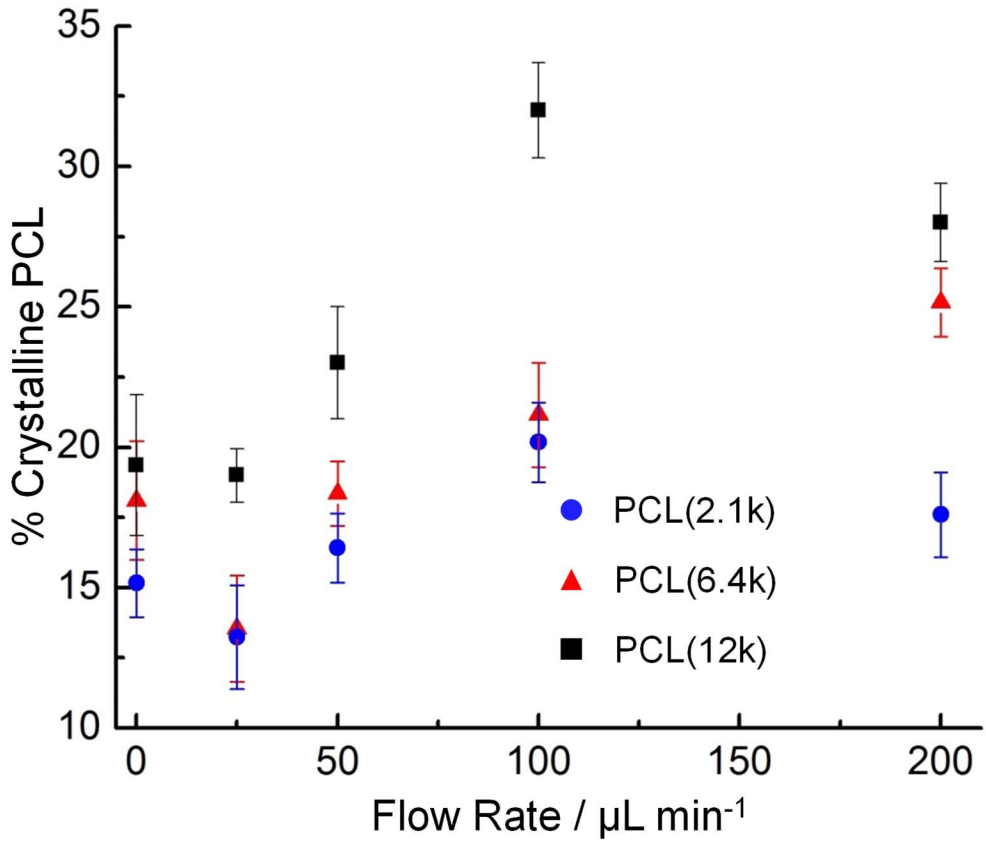

Figure 1. Effect of flow rate and copolymer composition on PCL crystallinity within the cores of PAX-loaded PCL-*b*-PEO PNPs.

We note that these trends in core crystallinity (Figure 2) show some correlation with the previously-discussed trends in PNP morphology (Figure 1). For example, for the bulk

preparations (Q = 0 μL/min), increasing crystallinity with increasing PCL block length (Figure 2) mirrors the decreasing curvature of the PNP morphologies (Figure 1, A, F and K). As for the microfluidic-prepared PNPs, increasing core crystallinity for the PCL(6.4k) copolymer with increasing flow rate (Figure 2) tracks with increasing numbers of cylindrical PNPs (Figure 1 G-J). Similarly, for the extreme block lengths (PCL(2.1k) and PCL(12k)), increasing core crystallinity with increasing flow rate (Figure 2) is concomitant with the formation of low curvature morphologies (Figure 1); however, a marked exception to the trend is found at the highest flow rate (Q = 200 μL/min), where a drop in core crystallinity accompanies the disappearance of cylindrical PNPs for both PCL(2.1k) and PCL(12k) copolymers (Figure 1 E and O, respectively).

The general increase in core crystallinity with increasing PCL block length at a given flow rate is expected, given that higher molecular weight polymers are known to show a stronger tendency to crystallize. On the other hand, the dependence of core crystallinity on flow rate is a result of shear-induced crystallization.[33] For most of the investigated flow rates, the core crystallinity of all three copolymers increased linearly with increasing flow rate, coinciding with the formation of low curvature PNP morphologies such as cylinders and lamellae. However, for the two extreme block lengths, the highest flow rate (Q = 200 μL/min) results in a surprising drop in core crystallinity (Figure 2), coinciding to a decrease in the size and curvature of PNPs (Figure 1 E and O). This result suggests that shear-induced breakup of large, low-curvature aggregates above a critical flow rate (Q = 200 μL/min for PCL(2.1k) and PCL(12k)) produces higher-curvature aggregates which in turn restricts chain crystallization. The same effect is not observed for the intermediate PCL block length (PCL(6.4k)), where both core crystallinity and low-curvature aggregate formation both steadily increase with flow rate up to the highest flow

rate of Q = 200 μL/min (Figure 2). We propose that the intermediate block length exhibits a balance of chain dynamics and crystallinity that leads to tougher aggregates which are less susceptible to shear-induced breakup than those formed from either PCL(2.1k) or PCL(12k).

Effect of Flow Rate and Block Copolymer Composition on PAX Loading Efficiencies. For the 15 PNP preparations at the same loading ratio of r = 0.01 described in the previous section (three different block copolymers and five different flow rates including the bulk preparations), PAX loading efficiencies were determined (Figure 2). For the bulk preparations,

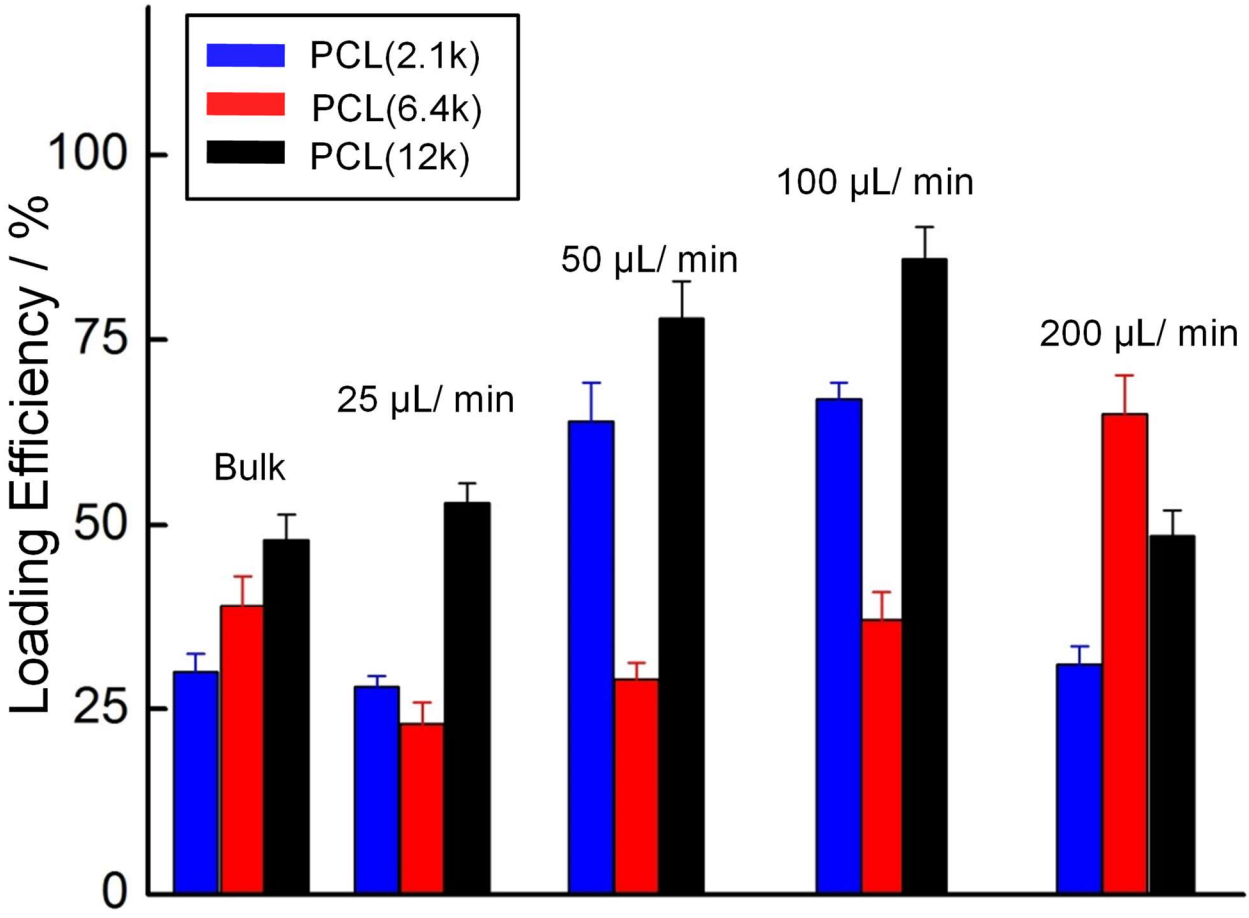

Figure 2. Effect of flow rate and water content on the loading efficiency of PAX-loaded PCL-*b*-PEO PNPs. Blue bars: PNPs prepared using PCL(2.1k); red bars: PNPs prepared using PCL(6.4k); and, black bars: PNPs prepared using PCL(12k).

loading efficiency increases as a function of increasing PCL block length as expected due to the increasing fraction of copolymer capable of solubilizing the hydrophobic drug. On the other hand, for the various microfluidic preparations, the same monotonic increase in loading efficiency with increasing PCL block length is not observed. For the first three flow rates (Q = 25 – 100 μL/min) we find that the loading efficiency decreases then increases as the PCL block length increases. On the other hand, at the highest flow rate (Q = 200 μL/min), the loading efficiency increases and then decreases as the PCL block length increases.

We next consider the effect of flow rate on loading efficiency for the various PCL block lengths. For the PCL(2.1k) copolymer (Figure 3, blue bars), loading efficiency is similar for the bulk (Q = 0 μL/min) and Q = 25 μL/min preparations, increases to similar loading efficiencies for the Q = 50 μL/min and Q = 100 μL/min preparations and then decreases for the Q = 200 μL/min preparation. For the PCL(6.4k) copolymer (Figure 3, red bars), loading efficiency decreases between the bulk and the Q = 25 μL/min preparation, and then increases steadily as the flow rate increases to Q = 200 μL/min. Finally, the PCL(12k) copolymer (Figure 3, black bars) shows a similar trend to the PCL(2.1k) copolymer, with loading efficiency being similar for the bulk and Q = 25 μL/min preparations, increasing to similar loading efficiencies for the Q = 50 μL/min and Q = 100 μL/min preparations and then decreasing for the Q = 200 μL/min preparation.

We note that these trends in PAX loading efficiency (Figure 3) track closely with trends in PCL crystallinity (Figure 2) and PNP size and morphology (Figure 1). Specifically, we find that for all three PCL block lengths, increasing PAX loading efficiency corresponds to increasing PCL core crystallinity and the formation of low internal curvature morphologies; furthermore, decreasing PAX loading efficiency corresponds to decreasing PCL core crystallinity and the

formation of mostly spherical PNPs. For example, considering the PCL(6.4) case (red triangles in Figure 2 and red bars in Figure 3), as the flow rate increases from Q = 0 μL/min (bulk preparation) to Q = 25 μL/min (microfluidic reactor), the crystallinity (Figure 2) and loading efficiency (Figure 3) both decrease, whereas further increases in flow rate in the microfluidic reactor from Q = 25 μL/min to Q = 200 μL/min leads to a steady increase in both crystallinity (Figure 2) and loading efficiency (Figure 3). The other two copolymers show similar correlations between crystallinities and loading efficiencies as flow rate increases. The observed correspondence between increasing core crystallinity and increasing PAX loading efficiency is opposite to what has been reported at higher PAX loading ratios where increasing PAX in the core is able to attenuate core crystallinity by disrupting copolymer chain packing, effectively acting as a plasticizer.[35] However, when PAX loading efficiency in Figure 3 is analyzed in the context of both PNP core crystallinity (Figure 2) and morphology (Figure 1), then the current trends can be understood. As discussed previously, the increases in crystallinity (Figure 2) are often associated with increases in the aggregate size (Figure 1),[32] which leads to larger hydrophobic core volumes for drug encapsulation (Figure 3). We have previously reported a similar trend for the PCL(12k) copolymer, also in the range of low loading ratio.[33] We conclude that there are two competing effects of core crystallization on the loading efficiency: one is to exclude drug from the crystallites, lowering the loading efficiency; the other is to increase the core volume, increasing the loading efficiency. It appears that the first effect is dominant at high loading ratios, as reported in ref. 35, and the latter effect is dominant at low loading levels, as reported here and in ref. 33.

Effect of Flow Rate and Block Copolymer Composition on PAX Release Kinetics. Diffusional PAX release kinetics were investigated for the three different block copolymer

compositions and five different flow rates (Figure 4). Two trends are apparent from these data: 1. for all three block copolymers, the bulk PNP formations show much faster PAX release than the microfluidic formulations, which show slower PAX release as the flow rate of microfluidic preparation increases; 2. PAX release becomes slower as the PCL block length increases; the same release data in Figure 4 is plotted to more clearly show this trend in Supporting Information, Figure S2.

Although it is uncertain why release rates in the bulk are faster than those obtained from microfluidic formulations, a possible explanation is that improved mixing in the microfluidic channels may lead to more uniform distributions of drug in the PCL cores. This proposal is based on the reasonable speculation that slow water addition may provide time for the drug to migrate to the core-corona interface, where it can undergo "burst" release, whereas fast microfluidic mixing may lead to sudden kinetic "freezing" of the drug in a more random distribution throughout the core. The general continued slowing of PAX release with increasing flow rate is likely due to the corresponding increase in shear-induced PCL crystallinity, which increases the core microviscosity and hence increases PAX diffusion times.[33] Compelling evidence for the relation between core crystallinity and PAX release rates comes from comparing changes to both properties when the flow rate increases from Q = 100 μL/min to Q = 200 μL/min for the three PCL block lengths; for the PCL(6.4k) copolymer, where the PCL crystallinity steadily increases in this range (Figure 2), the PAX release rate becomes concomitantly slower (Figure 4B), whereas for the other two PCL blocks, where the PCL crystallinity does not increase and in fact decreases (Figure 2), there is no corresponding slowing of the PAX release rate (Figure 4, A and C). Moreover, the slowing of release rates with increasing PCL block length for each flow rate (Supporting Information, Figure S2) is also explained in terms of PNP core crystallinity.

Specifically, PCL crystallinity at each flow rate is found to increase as the PCL block length increases (Figure 2). Again, an increase in PCL crystallization slows the diffusional release kinetics of encapsulated PAX molecules by increasing the microviscosity of the PCL core, as shown in our previous study.[33]

Although we have not yet done a systematic study of the effect of polydispersity on release rates, we point out that our data in no way suggests that polydispersity does not affect release rates, despite the high reproducibility of the percentage PAX release values over three replicate preparations. Microfluidic preparations in the two-phase reactor tend to very reproducible in terms of morphologies, mean sizes and mean ensemble parameters such as crystallinity, loading efficiency, and percentage drug release after release time *t*.[33-35, 41-43, 45-49] This does not mean that the samples are not polydisperse (they clearly are). It only means that the polydispersity and mean parameters are reproducible under a given set of preparation conditions. Clearly the mean release percentages will be a convolution of release percentages from many particle morphologies and sizes within the distribution, but unfortunately we cannot separate contributions from the various distribution fractions using the current mean values. Future experiments to probe how size, shape and crystallinity polydispersity within PNP distributions affects various mean drug delivery parameters will be the subject of future studies in our group.

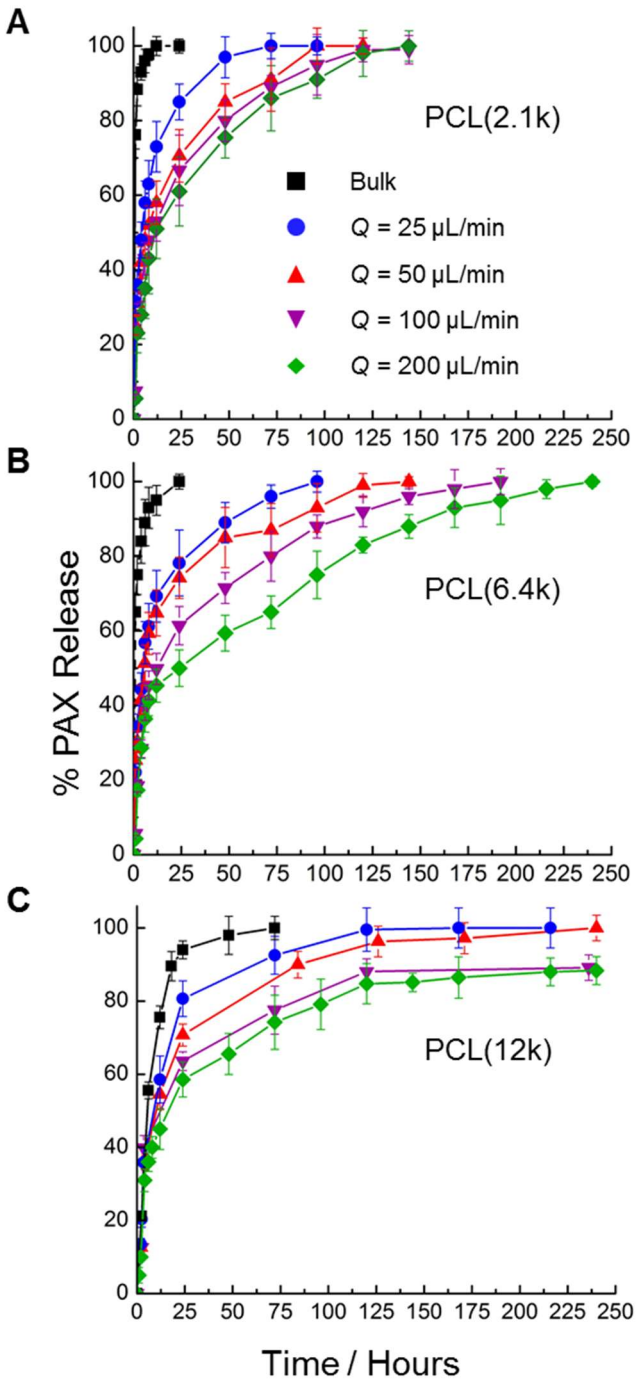

Figure 3. Effect of flow rate and PCL block length on the release profiles of PAX from PAX-loaded PCL-*b*-PEO PNPs. Release profiles for PNPs prepared using various flow rates from (A) PCL(2.1k), (B) PCL(6.4k), and (C) PCL(12k).

Effect of Drug Loading Ratio on Multiscale Structure, PAX Loading Efficiencies, and PAX Release Kinetics. Next, we explored the effect of drug loading ratio on sizes and morphologies of PNPs prepared using microfluidics. For this study we investigated four different drug loading ratios (all less than the r = 0.01 case used in previous sections) spanning two full orders of magnitude (r = 0.005, 0.001, 0.0005, and 0.0001). For these PNP preparations, a single block copolymer was used (PCL(12k)) and the microfluidic flow rate was held constant at Q =

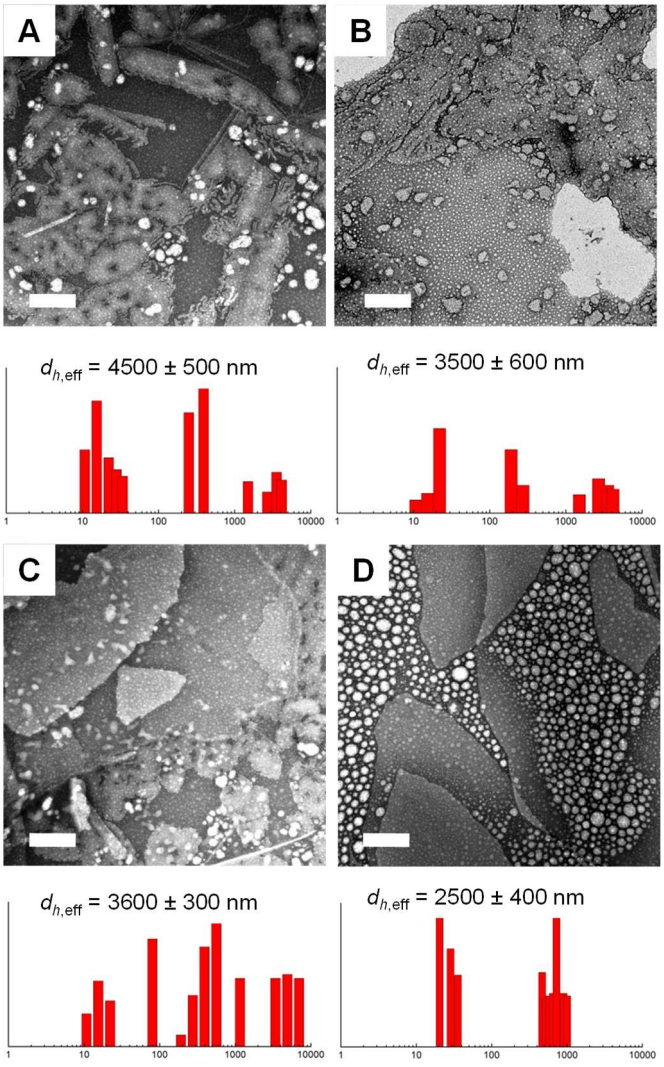

Figure 4. Effect of drug-to-copolymer ratio on the morphologies and hydrodynamic sizes of PAX-loaded PNPs. TEM images and corresponding intensity distributions determined by inverse Laplace (CONTIN) analysis with mean effective hydrodynamic diameters determined from cumulant analysis, for PNPs prepared from PCL(12k) at Q = 50 μL/min and (A) r = 0.005, (B) r = 0.001, (C) r = 0.0005, and (D) r = 0.0001. All scale bars are 200 nm.

50 μL/min.

TEM images and DLS size distributions of the resulting PNP samples are shown in Figure 5. The TEM data shows that qualitative morphologies do not vary strongly in this range of *r*, with all drug loading ratios between $r = 0.005$ and $r = 0.0005$ yielding a mixture of spheres, cylinders and lamellae (Figure 5, A-C). However, when the loading ratio drops to $r = 0.0001$, cylinders are no longer formed and only a mixture of spheres and lamellae are observed (Figure 5D). We also find a steady decrease in the mean effective hydrodynamic diameter from DLS measurements, from 4500 nm to 2500 nm as the loading ratio is decreased from $r = 0.005$ to $r = 0.0001$. These results indicate small but notable effects of PNP size and morphologies for extremely low loading ratios, down to relative drug mass $1/100^{th}$ of a percent of the copolymer mass ($r = 0.0001$).

Despite the observed effects of loading ratio on the size and structure on colloidal length scales, we find no significant corresponding effects of *r* on the crystallinity and loading efficiency in this regime of extremely low loading ratios. Figure 6 shows that differences in loading efficiencies (91 - 94 %) and percentages of crystalline PCL (40 – 50 %) across the range of $r = 0.005$-0.0001 fall within the experimental error and therefore are not significant. These data suggest that loading ratios do not significantly affect the internal microstructure of PNPs in this range of extremely low loading ratios ($r \leq 0.01$) in contrast to the previous-reported marked effects of loading ratio on loading efficiency and PCL crystallinity when the PAX loading ratio is much higher ($r \geq 0.1$).[35]

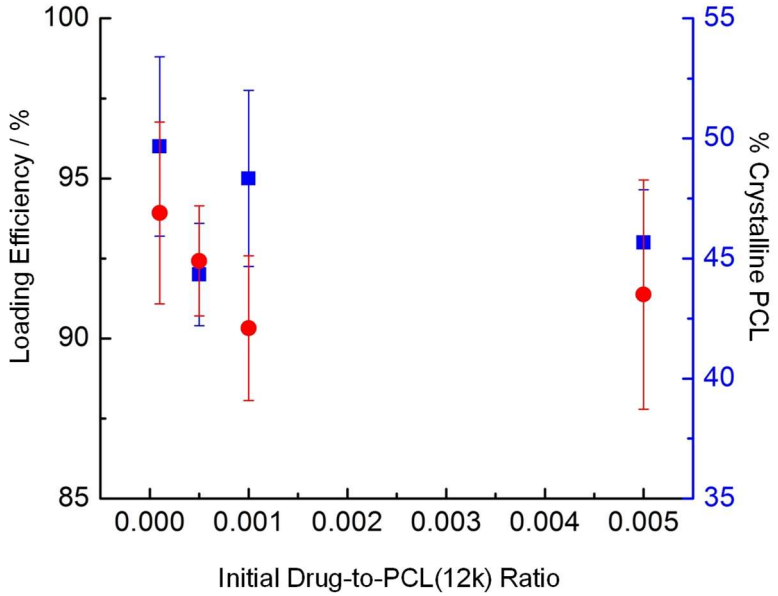

Figure 6. Effect of drug loading ratio *r* on PCL crystallinity (blue squares) and PAX loading efficiency (red circles) of PAX-loaded PNPs. All samples were prepared using PCL(12k) copolymer compositions, at Q = 50 μL/min.

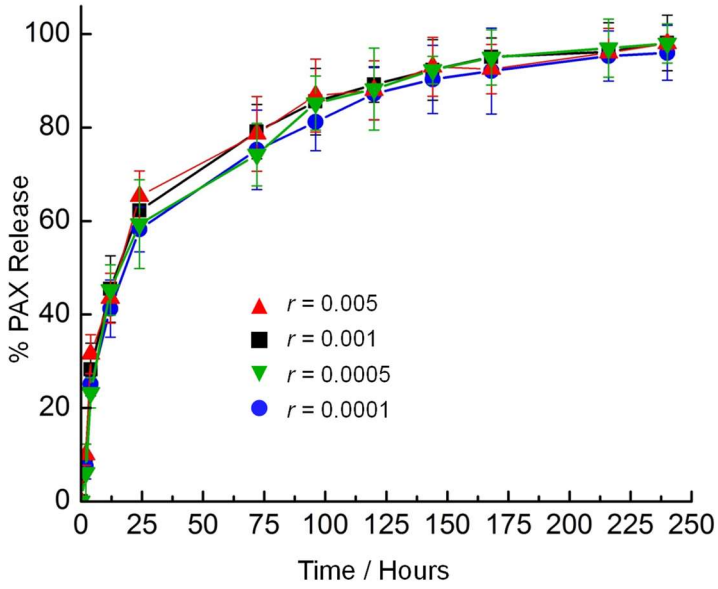

Figure 5. Effect of drug loading ratio on PAX release profiles of PAX-loaded PNPs. All samples were prepared using PCL(12k) copolymer compositions, at Q = 50 μL/min.

Finally, Figure 5 shows that PAX release profiles for the four different loading ratios are effectively the same with no significant differences within experimental error. For all four formulations, complete PAX release occurred over ~10 days following nearly identical release profiles. These data suggest that the release profiles are governed primarily by the microstructure (internal crystallinity and loading levels, Figure 6) which are the same for the different loading ratios, and not by the morphologies and colloidal sizes (Figure 5) which show small differences as the loading ratio is varied in this range of $r < 0.01$.

Conclusion

The application of external forces (e.g. shear or confinement) within microfluidic reactors and other microstructured environments to directing the size, morphology and internal crystallinity of polymeric nanoparticles for drug delivery provides promising routes to controlling nanomedicines through processing at the nanoscale.[33-35,41-43] In this paper, we prepared PAX-loaded PNPs both in the bulk and in a two-phase microfluidic reactor at variable flow rate, and studied the effects of flow rate, copolymer composition and PAX loading ratio on the multiscale structure, loading efficiency and PAX release rate. These experiments were undertaken in the limit of low loading ratios ($r \leq 0.01$), much lower than PAX loading ratios previously investigated in our group,[33,35] where we show that PCL crystallinity, loading efficiency and release rate are not found to be significantly affected by the amount of PAX dissolved in the core over a two order of magnitude variation in the PAX loading ratio. These results are in sharp contrast to our recent study of microfluidic PNPs prepared in a range of high loading ratios ($r \geq 0.1$), where the amount of added PAX has a strong influence on the multiscale structure and properties of drug delivery PNPs.[35] This work thus enables deconvolution of

processing effects on the structure and function of PNPs from perturbations caused by the added molecular cargo, providing critical insights for the preparation of more medically-relevant PNPs at higher therapeutic loading levels. In addition, we show that PCL crystallinity, loading efficiency and release rate are strongly dependent on both the microfluidic flow rate and the block copolymer composition. This suggests that both variables provide complementary chemical and processing handles for reproducible tuning of structure and function of PAX-loaded PNPs.

Supporting Information. DLS size distributions corresponding to TEM data in Figure 1; PAX release profiles plotted to compare effect of PCL block length at various flow rates; Comparison of PNP morphologies with (I) and without (II) quenching and dialysis after collection from the microfluidic reactor.

Acknowledgements. We are grateful to the Natural Sciences and Engineering Research Council of Canada, NSERC, for financial support. We acknowledge Dr. Patrick Nahirney and the UVic EM lab (Department of Biology) for the continued use of their TEM. We are also grateful to Prof. David Sinton and Dr. Jason Riordon (University of Toronto) for valuable discussions.

References

(1) Allen, C.; Maysinger, D.; Eisenberg, A. Nano-engineering block copolymer aggregates for drug delivery. *Colloids and Surfaces B: Biointerfaces* **1999**, *16*, 3-27.

(2) Discher, D. E.; Ortiz, V.; Srinivas, G.; Klein, M. L.; Kim, Y.; Christian, D.; Cai, S.; Photos, P.; Ahmed, F. Emerging Applications of Polymersomes in Delivery: from Molecular Dynamics to Shrinkage of Tumors. *Prog Polym Sci* **2007**, *32*, 838-857.

(3) Branco, M. C.; Schneider, J. P. Self-assembling materials for therapeutic delivery. *Acta biomaterialia* **2009**, *5*, 817-831.

(4) Tyrrell, Z. L.; Shen, Y. Q.; Radosz, M. Fabrication of micellar nanoparticles for drug delivery through the self-assembly of block copolymers. *Prog Polym Sci* **2010**, *35*, 1128-1143.

(5) Gong, J.; Chen, M. W.; Zheng, Y.; Wang, S. P.; Wang, Y. T. Polymeric micelles drug delivery system in oncology. *Journal of Controlled Release* **2012**, *159*, 312-323.

(6) Kataoka, K.; Harada, A.; Nagasaki, Y. Block copolymer micelles for drug delivery: Design, characterization and biological significance. *Adv Drug Deliver Rev* **2012**, *64*, 37-48.

(7) Parveen, S.; Misra, R.; Sahoo, S. K. Nanoparticles: a boon to drug delivery, therapeutics, diagnostics and imaging. *Nanomed-Nanotechnol* **2012**, *8*, 147-166.

(8) Lee, J. S.; Feijen, J. Polymersomes for drug delivery: Design, formation and characterization. *Journal of Controlled Release* **2012**, *161*, 473-483.

(9) Kwon, G. S.; Kataoka, K. Block copolymer micelles as long-circulating drug vehicles. *Adv Drug Deliver Rev* **2012**, *64*, 237-245.

(10) Rosler, A.; Vandermeulen, G. W. M.; Klok, H. A. Advanced drug delivery devices via self-assembly of amphiphilic block copolymers. *Adv Drug Deliver Rev* **2012**, *64*, 270-279.

(11) Elsabahy, M.; Wooley, K. L. Design of polymeric nanoparticles for biomedical delivery applications. *Chemical Society Reviews* **2012**, *41*, 2545-2561.

(12) Zhang, Y.; Chan, H. F.; Leong, K. W. Advanced materials and processing for drug delivery: The past and the future. *Adv Drug Deliver Rev* **2013**, *65*, 104-120.

(13) Nicolas, J.; Mura, S.; Brambilla, D.; Mackiewicz, N.; Couvreur, P. Design, functionalization strategies and biomedical applications of targeted biodegradable/biocompatible polymer-based nanocarriers for drug delivery. *Chemical Society Reviews* **2013**, *42*, 1147-1235.

(14) Lu, Y.; Park, K. Polymeric micelles and alternative nanonized delivery vehicles for poorly soluble drugs. *Int J Pharmaceut* **2013**, *453*, 198-214.

(15) Ahmad, Z.; Shah, A.; Siddiq, M.; Kraatz, H. B. Polymeric micelles as drug delivery vehicles. *Rsc Adv* **2014**, *4*, 17028-17038.

(16) Oltra, N. S.; Nair, P.; Discher, D. E. From Stealthy Polymersomes and Filomicelles to "Self" Peptide-Nanoparticles for Cancer Therapy. *Annu Rev Chem Biomol* **2014**, *5*, 281-299.

(17) Sun, T.; Zhang, Y. S.; Pang, B.; Hyun, D. C.; Yang, M.; Xia, Y. Engineered nanoparticles for drug delivery in cancer therapy. *Angewandte Chemie International Edition* **2014**, *53*, 12320-12364.

(18) Yokoyama, M. Polymeric micelles as drug carriers: their lights and shadows. *Journal of drug targeting* **2014**, *22*, 576-583.

(19) Prabhu, R. H.; Patravale, V. B.; Joshi, M. D. Polymeric nanoparticles for targeted treatment in oncology: current insights. *Int J Nanomed* **2015**, *10*, 1001-1018.

(20) Ulbrich, K.; Hola, K.; Subr, V.; Bakandritsos, A.; Tucek, J.; Zboril, R. Targeted Drug Delivery with Polymers and Magnetic Nanoparticles: Covalent and Noncovalent Approaches, Release Control, and Clinical Studies. *Chem Rev* **2016**, *116*, 5338-5431.

(21) Zhang, K. R.; Tang, X.; Zhang, J.; Lu, W.; Lin, X.; Zhang, Y.; Tian, B.; Yang, H.; He, H. B. PEG-PLGA copolymers: Their structure and structure-influenced drug delivery applications. *Journal of Controlled Release* **2014**, *183*, 77-86.

(22) Letchford, K.; Liggins, R.; Wasan, K.; Burt, H. In vitro human plasma distribution of nanoparticulate paclitaxel is dependent on the physicochemical properties of poly(ethylene glycol)-block-poly(caprolactone) nanoparticles. *Eur J Pharm Biopharm* **2009**, *71*, 196-206.

(23) Glover, A. L.; Nikles, S. M.; Nikles, J. A.; Brazel, C. S.; Nikles, D. E. Polymer micelles with crystalline cores for thermally triggered release. *Langmuir* **2012**, *28*, 10653-10660.

(24) Cai, S.; Vijayan, K.; Cheng, D.; Lima, E. M.; Discher, D. E. Micelles of different morphologies--advantages of worm-like filomicelles of PEO-PCL in paclitaxel delivery. *Pharmaceutical research* **2007**, *24*, 2099-2109.

(25) Geng, Y.; Dalhaimer, P.; Cai, S.; Tsai, R.; Tewari, M.; Minko, T.; Discher, D. E. Shape effects of filaments versus spherical particles in flow and drug delivery. *Nat Nanotechnol* **2007**, *2*, 249-255.

(26) Fairley, N.; Hoang, B.; Allen, C. Morphological Control of Poly(ethylene glycol)-block-poly(eta-caprolactone) Copolymer Aggregates in Aqueous Solution. *Biomacromolecules* **2008**, *8*, 2283-2291.

(27) Venkataraman, S.; Hedrick, J.; Ong, Z.; Yang, C.; Ee, P.; Hammond, P.; Yang, Y. The effects of polymeric nanostructure shape on drug delivery. *Adv Drug Deliver Rev* **2011**, *63*, 1228-1246.

(28) Gaumet, M.; Vargas, A.; Gurny, R.; Delie, F. Nanoparticles for drug delivery: The need for precision in reporting particle size parameters. *Eur J Pharm Biopharm* **2008**, *69*, 1-9.

(29) Truong, N. P.; Whittaker, M. R.; Mak, C. W.; Davis, T. P. The importance of nanoparticle shape in cancer drug delivery. *Expert Opin Drug Del* **2015**, *12*, 129-142.

(30) Du, Z. X.; Xu, J. T.; Fan, Z. Q. Micellar morphologies of poly(epsilon-caprolactone)-b-poly(ethylene oxide) block copolymers in water with a crystalline core. *Macromolecules* **2007**, *40*, 7633-7637.

(31) Du, Z. X.; Xu, J. T.; Fan, Z. Q. Regulation of micellar morphology of PCL-b-PEO block copolymers by crystallization temperature. *Macromol Rapid Comm* **2008**, *29*, 467-471.

(32) Rizis, G.; van de Ven, T. G. M.; Eisenberg, A. Crystallinity-driven morphological ripening processes for poly(ethylene oxide)-block-polycaprolactone micelles in water. *Soft Matter* **2014**, *10*, 2825-2835.

(33) Bains, A.; Cao, Y. M.; Moffitt, M. G. Multiscale Control of Hierarchical Structure in Crystalline Block Copolymer Nanoparticles Using Microfluidics. *Macromol Rapid Comm* **2015**, *36*, 2000-2005.

(34) Bains, A.; Wulff, J. E.; Moffitt, M. G. Microfluidic synthesis of dye-loaded polycaprolactone-block-poly (ethylene oxide) nanoparticles: Insights into flow-directed loading and in vitro release for drug delivery. *J Colloid Interf Sci* **2016**, *475*, 136-148.

(35) Bains, A.; Cao, Y. M.; Kly, S.; Wulff, J. E.; Moffitt, M. G. Controlling structure and function of polymeric drug delivery nanoparticles using microfluidics. *Molecular pharmaceutics* **2017**, in press.

(36) Zhang, L.; Eisenberg, A. Multiple Morphologies of "Crew-Cut" Aggregates of Polystyrene-b-poly(acrylic acid) Block Copolymers. *Science* **1995**, *268*, 1728-1731.

(37) Zhang, L.; Eisenberg, A. Multiple Morphologies and Characteristics of "Crew-Cut" Micelle-like Aggregates of Polystyrene-b-poly(acrylic acid) Diblock Copolymers in Aqueous Solutions. *J Am Chem Soc* **1996**, *118*, 3168-3181.

(38) Yu, Y. S.; Eisenberg, A. Control of morphology through polymer-solvent interactions in crew-cut aggregates of amphiphilic block copolymers. *J Am Chem Soc* **1997**, *119*, 8383-8384.

(39) Zhang, L.; Yu, K.; Eisenberg, A. Ion-Induced Morphological Changes in ``Crew-Cut" Aggregates of Amphiphilic Block Copolymers. *Science* **1996**, *272*, 1777-1779.

(40) Zhang, L. E., A. Morphogenic Effect of Added Ions on Crew-Cut Aggregates of Polystyrene-b-poly(acrylic acid) Block Copolymers in Solutions. *Macromolecules* **1996**, *29*, 8805-8815.

(41) Schabas, G.; Wang, C. W.; Oskooei, A.; Yusuf, H.; Moffitt, M. G.; Sinton, D. Formation and shear-induced processing of quantum dot colloidal assemblies in a multiphase microfluidic chip. *Langmuir* **2008**, *24*, 10596-10603.

(42) Wang, C. W.; Oskooei, A.; Sinton, D.; Moffitt, M. G. Controlled Self-Assembly of Quantum Dot-Block Copolymer Colloids in Multiphase Microfluidic Reactors. *Langmuir* **2010**, *26*, 716-723.

(43) Wang, C. W.; Sinton, D.; Moffitt, M. G. Flow-Directed Block Copolymer Micelle Morphologies via Microfluidic Self-Assembly. *J Am Chem Soc* **2011**, *133*, 18853-18864.

(44) Gunther, A.; Khan, S. A.; Thalmann, M.; Trachsel, F.; Jensen, K. F. Transport and reaction in microscale segmented gas-liquid flow. *Lab Chip* **2004**, *4*, 278-286.

(45) Wang, C. W.; Bains, A.; Sinton, D.; Moffitt, M. G. Flow-Directed Assembly of Block Copolymer Vesicles in the Lab-on-a-Chip. *Langmuir* **2012**, *28*, 15756-15761.

(46) Wang, C. W.; Sinton, D.; Moffitt, M. G. Morphological Control via Chemical and Shear Forces in Block Copolymer Self-Assembly in the Lab-on-Chip. *Acs Nano* **2013**, *7*, 1424-1436.

(47) Wang, C. W.; Bains, A.; Sinton, D.; Moffitt, M. G. Flow-Directed Loading of Block Copolymer Micelles with Hydrophobic Probes in a Gas-Liquid Microreactor. *Langmuir* **2013**, *29*, 8385-8394.

(48) Xu, Z. Q.; Yan, B.; Riordon, J.; Zhao, Y.; Sinton, D.; Moffitt, M. G. Microfluidic Synthesis of Photoresponsive Spool-Like Block Copolymer Nanoparticles: Flow-Directed Formation and Light-Triggered Dissociation. *Chem Mater* **2015**, *27*, 8094-8104.

(49) Xu, Z. Q.; Lu, C. H.; Riordon, J.; Sinton, D.; Moffitt, M. G. Microfluidic Manufacturing of Polymeric Nanoparticles: Comparing Flow Control of Multiscale Structure in

Single-Phase Staggered Herringbone and Two-Phase Reactors. *Langmuir* **2016**, *32*, 12781-12789.

(50) Šachl, R.; Uchman, M.; Matějíček, P.; Procházka, K.; Štěpánek, M.; Špírková, M. Preparation and Characterization of Self-Assembled Nanoparticles Formed by Poly (ethylene oxide)-block-poly (ε-caprolactone) Copolymers with Long Poly (ε-caprolactone) Blocks in Aqueous Solutions. *Langmuir* **2007**, *23*, 3395-3400.

(51) Šachl, R.; Štěpánek, M.; Procházka, K.; Humpolíčková, J.; Hof, M. Fluorescence study of the solvation of fluorescent probes prodan and laurdan in poly (ε-caprolactone)-block-poly (ethylene oxide) vesicles in aqueous solutions with tetrahydrofurane. *Langmuir* **2008**, *24*, 288-295.

(52) Dionzou, M.; Morère, A.; Roux, C.; Lonetti, B.; Marty, J.-D.; Mingotaud, C.; Joseph, P.; Goudounèche, D.; Payré, B.; Léonetti, M. Comparison of methods for the fabrication and the characterization of polymer self-assemblies: what are the important parameters? *Soft Matter* **2016**, *12*, 2166-2176.

(53) Qi, W.; Ghoroghchian, P. P.; Li, G.; Hammer, D. A.; Therien, M. J. Aqueous self-assembly of poly (ethylene oxide)-block-poly (ε-caprolactone)(PEO-b-PCL) copolymers: disparate diblock copolymer compositions give rise to nano-and meso-scale bilayered vesicles. *Nanoscale* **2013**, *5*, 10908-10915.

(54) Zhang, L.; Eisenberg, A. Thermodynamic vs Kinetic Aspects in the Formation and Morphological Transitions of Crew-Cut Aggregates Produced by Self-Assembly of Polystyrene-b-poly(acrylic acid) Block Copolymers in Dilute Solution. *Macromolecules* **1999**, *32*, 2239-2249.

(55) Harris, J. R.; Roos, C.; Djalali, R.; Rheingans, O.; Maskos, M.; Schmidt, M. Application of the negative staining technique to both aqueous and organic solvent solutions of polymer particles. *Micron* **1999**, *30*, 289-298.

TOC graphic